REPORT DOCUMENTATION PAGE

Form Approved
OMB No. 0704-0188

1. REPORT DATE *(DD-MM-YYYY)*	2. REPORT TYPE	3. DATES COVERED *(From - To)*
May 2002	Conference Proceedings	1/00 - 5/02

4. TITLE AND SUBTITLE
Recent Progress in the Development of a Multi-Watt All Gas-Phase Iodine Laser (AGIL)

5a. CONTRACT NUMBER

5b. GRANT NUMBER

5c. PROGRAM ELEMENT NUMBER

6. AUTHOR(S)
Gerald C. Manke II, Thomas L. Henshaw, Chris B. Cooper, Gordon D. Hager

5d. PROJECT NUMBER
3326

5e. TASK NUMBER
LA

5f. WORK UNIT NUMBER
02

7. PERFORMING ORGANIZATION NAME(S) AND ADDRESS(ES)

Air Force Research Laboratory
Directed Energy Directorate
3550 Aberdeen Ave. SE
Kirtland AFB, NM 87117

8. PERFORMING ORGANIZATION REPORT NUMBER

9. SPONSORING / MONITORING AGENCY NAME(S) AND ADDRESS(ES)
Air Force Research Laboratory
Directed Energy Directorate
3550 Aberdeen Ave. SE
Kirtland AFB, NM 87117

10. SPONSOR/MONITOR'S ACRONYM(S)

11. SPONSOR/MONITOR'S REPORT NUMBER(S)

12. DISTRIBUTION / AVAILABILITY STATEMENT
Approved for public release; distribution is unlimited

13. SUPPLEMENTARY NOTES
Proceedings of the 33rd AIAA Plasmadynamics and Lasers Conference
AIAA-2002-2126

14. ABSTRACT
Recent results in the development of a multi-watt All Gas-phase Iodine Laser (AGIL) are presented. A description of the subsonic hardware used to produce NCl(a), direct measurements of the I* - I small signal gain and parametric studies to optimize the gain are described.

15. SUBJECT TERMS
AGIL, chemical iodine lasers

16. SECURITY CLASSIFICATION OF:			17. LIMITATION OF ABSTRACT	18. NUMBER OF PAGES	19a. NAME OF RESPONSIBLE PERSON
a. REPORT	b. ABSTRACT	c. THIS PAGE			Gerald C. Manke II
Unclassified	Unclassified	Unclassified	Unlimited	12	19b. TELEPHONE NUMBER *(include area code)* 505-853-2674

2002-2126

RECENT PROGRESS IN THE DEVELOPMENT OF A MULTI-WATT ALL GAS-PHASE IODINE LASER (AGIL)*

Gerald C. Manke II[†a], Thomas L. Henshaw[b], Chris B. Cooper[c], and Gordon D. Hager[a]
[a]Air Force Research Laboratory, Directed Energy Directorate, Kirtland AFB, NM 87117
[b] Directed Energy Solutions, Colorado Springs, CO 80921
[c] Boeing-Rocketdyne, Kirtland AFB, NM 87117

ABSTRACT

Recent results in the development of a multi-watt All Gas-phase Iodine Laser (AGIL) are presented. A description of the subsonic hardware used to produce $NCl(a^1\Delta)$, direct measurements of $I^*(^2P_{1/2})$ - $I(^2P_{3/2})$ small signal gain, and parametric studies to optimize the gain are described.

INTRODUCTION

Since the invention of the COIL laser in the mid-1970's[1], there has been interest in alternative energy carrier molecules that react via energy transfer with ground state iodine atoms to generate an inversion on the electronic spin-orbit transition:

$$O_2(a^1\Delta) + I \rightarrow O_2(X^3\Sigma^-) + I^*(^2P_{1/2}) \qquad [1]$$

In principle, all molecules with the $(p\pi^*)^2$ $(p\sigma^*)^0$ electronic configuration will have the same electronic states as O_2, ie. $(X^3\Sigma^-)$, $(a^1\Delta)$, and $(b^1\Sigma^+)$. Because of the selection rules for electronic transitions, the singlet delta state is metastable. The singlet nitrenes, in particular (ie. NF, NCl) have been investigated as possible replacements or alternatives to $O_2(a^1\Delta)$ because they share they have the requisite $(p\pi^*)^2$ $(p\sigma^*)^0$ electronic configuration[2]. These metastable molecules have radiative lifetimes in the 2 - 5 s range[3-5] and have the potential to be useful energy carriers in energy transfer chemical laser applications.

Unfortunately, metastability is not the only figure of merit for chemical laser devices based on an energy transfer process. The ability to transfer energy to a suitable laser species (such as iodine atoms) depends on the detailed kinetics and dynamics of the interaction between the energy donor and acceptor, which are determined by the details of the complex multidimensional potential energy surfaces that govern the interaction[2].

To date, only $NF(a^1\Delta)$ and $NCl(a^1\Delta)$ have been found to have the properties necessary to serve as energy carriers. Namely, both have long radiative lifetimes and are relatively inert to chemical reaction and physical quenching[6, 7]. Indeed, there have been several demonstrations of efficient energy transfer from $NF(a^1\Delta)$ to Bi[8, 9], BiF[10-12], and BH[13-15]. Unfortunately, these systems were not suitable for generating high-energy chemical lasers[2]. Attempts to generate an $NF(a^1\Delta)$ / I energy transfer laser have also failed[16]. The reason for this failure is that despite the fast reaction of $NF(a^1\Delta)$ with atomic iodine ($k_2 = 1.8 \pm 0.4 \times 10^{-11}$ cm^3 molecule^{-1} s^{-1})[17]

$$NF(a^1\Delta) + I \rightarrow NF(X^3\Sigma^-) + I^* \qquad [2a]$$
$$\rightarrow \text{products} \qquad [2b]$$

an inversion is prevented by a poor branching fraction for [2a] (~10-20%)[18, 19] and fast quenching of I^* by $NF(a^1\Delta)$ (k_3=5.7 x 10^{-11} cm^3 molecules^{-1} s^{-1})[17, 20]

$$NF(a^1\Delta) + I^* \rightarrow NF(b^1\Sigma^+) + I(^2P_{3/2}) \qquad [3].$$

On the other hand, $NCl(a^1\Delta)$ not only has a fast quenching reaction with atomic iodine ($k_4 = 1.5 \pm 0.7$ x 10^{-11} cm^3 molecules^{-1} s^{-1})[21, 22],

$$NCl(a^1\Delta) + I \rightarrow NCl(X^3\Sigma^-) + I^* \qquad [4a]$$
$$\rightarrow \text{products} \qquad [4b]$$

but the branching fraction for $I^*(^2P_{3/2})$ formation is large ($\Gamma \geq 0.7$) and the energy pooling reaction between $NCl(a^1\Delta)$ and $I^*(^2P_{1/2})$ does not appear to be important. Hence, $NCl(a^1\Delta)$ should be an efficient energy carrier suitable for a scalable energy transfer chemical iodine laser.

---

* This paper is declared a work of the U.S. Government and is not subject to copyright protection in the United States.

† Corresponding author

Indeed, a subsonic, continuous wave, chemical $I^*(^2P_{1/2})$ laser pumped by $NCl(a^1\Delta)$ was reported by Henshaw and co-workers in 2000[23]. The authors named their discovery the All Gas-phase Iodine Laser, or AGIL. Their demonstration was motivated and enabled by the small signal gain measurements of Herbelin, et. al.[24], Bower et. al.[25], and the transient lasing demonstration of Ray and Coombe[26]. Other milestones in the history of AGIL are discussed in detail elsewhere[2].

Since the initial, sub-watt laser demonstration there has been considerable effort expended to scale this device to multi-watt powers, and to design an AGIL device that uses technology suitable for high power applications. This report summarizes the results of these experiments and reviews the prospects of generating a multi-watt AGIL device.

EXPERIMENTAL METHODS

A new subsonic flow device for the generation of $NCl(a^1\Delta)$ was constructed following the completion of the work that culminated in the demonstration of a 180mW AGIL device. The new reactor (AGIL 2) is very similar in design to the old device (AGIL 1)[23,24,27] in terms of materials, geometry, and injector locations. The most significant changes are the optical path length was increased to 20 cm(as opposed to 5 cm), F atoms are produced by four discharge tubes (as opposed to one), and the purge flows along the sides of the reactor were improved to provide better containment of the main flow. A construction schematic of AGIL 2 is shown in Figure 1. The flow channel height in he injector block section can be set at either 2.0 or 1.0 cm and the separation between the HI and HN_3 injectors can be changed from 1.3 cm to 5.0 cm. A small amount of area relief is provided by an adjustable ramp that can expand from 5 to 10 degrees. The experiments described here reproduce the AGIL 1 device geometry and use the 2.0 cm high flow channel, 1.3 cm separation between the HI and HN_3 injectors, and a 7-degree expansion.

The four discharge tubes are powered by a new power supply (10 kV and 3.5 Amps maximum per tube) and cooled by chilled water. Fluorine atoms are generated when NF_3 or F_2 are passed through the discharge. The maximum current from the power supply used for AGIL 1 was 2.5A (10 kV). This supply was powerful enough to fully dissociate 1 mmol sec^{-1} of F_2 or 1.5 mmol sec^{-1} of NF_3. In both cases, approximately 2 mmol s^{-1} of F atoms are generated. Higher flow rates of F_2 led to incomplete dissociation, while higher flow rates of NF_3 extinguished the discharge. NF_3 is the preferred F atom source because no molecular F_2 is present in the flow and subsequent reactions with Cl and I to generate IF and ClF (both are strong quenchers of $I^*(^2P_{1/2})$ and $NCl(a^1\Delta)$) are prevented. The new power supply allows for higher F_2 and NF_3 flow rates, and yields larger F atom flows than previously generated in AGIL 1[27].

Helium and deuterium chloride are added through radial injectors at the end of each discharge tube to convert the flow of F atoms to Cl. Hydrogen iodide and hydrogen azide are cross-injected into the flow 6.6 and 7.9 cm downstream, respectively. Each HI injector block consists of a row of 168 holes with a diameter of 0.030 cm and a row of 84 holes with a diameter of 0.066 cm. Each HN_3 injector block consists of a row of 184 holes with a diameter of 0.025 cm and a row of 96 holes with a diameter of 0.050 cm. The effective HN_3 injector area (including both the top and bottom injector blocks) is 0.58 cm^2 (0.86 cm effective diameter) and the effective HI injector area is 0.82 cm^2 (1.02 cm effective diameter).

The discharge efficiency was characterized according to the titration methods described by Manke and co-workers[27], see below. Initially, gas-phase titrations were performed by measuring the yield of I atoms with a tunable diode laser that probes the 1.315 micron $I(^2P_{3/2})$ - $I^*(^2P_{1/2})$, F(3,4) spin-orbit transition. As the difficulty of maintaining high flows of HI increased and the cost of HI became prohibitive, the titration technique was altered by adding HCl as the titrant and monitoring the relative concentration of HF(v = 0) via absorption on nearby HF(2-0) ro-vibrational transitions. To expedite data collection, the diode laser output was split into three beams that probed three streamwise positions along the reactor. Small signal gain measurements were performed as previously described by Herbelin, et. al[24].

Table 1 compares the typical experimental conditions used in this study to those from AGIL 1. The flow rate values in parentheses in the first and second columns are Herbelin's[24] and Henshaw's[23] values multiplied by 4. Since the AGIL 2 device is essentially 4 times larger than AGIL 1, these are the target values for our study. All gas flows were controlled in the same manner as for AGIL 1 previously.

Table 1: Typical Experimental Conditions

Species	Flow Rates (mmol s^{-1})		
	AGIL 1 (Herbelin)[24]	AGIL 1 (Henshaw)[23]	AGIL 2 (this work)
He	150 (600)	130 - 150 (520 - 600)	480 - 1000
NF_3	NA	1 - 1.5 (4 - 6)	4 - 16
F_2	0.66 (2.64)	NA	2 - 6
DCl	2.0 (8.0)	2.0 - 2.5 (8 - 10)	16 - 25
HI	0.032 (0.12)	0.04 - 0.07 (0.16 - 0.28)	0.12 - 0.16
HN_3	3.32 (13.3)	3 - 4.5 (12 - 18)	10 - 50
Pressure (Torr)	16	15 - 16	12 - 24

EXPERIMENTAL RESULTS

F atom titrations

A series of typical F atom titration plots are shown in Figure 2, where the flow rate of atomic iodine and temperature are plotted as a function of added HI at three streamwise positions. Titrations are shown for NF_3 = 4 and 6 mmol s^{-1}, and F_2 = 4 and 6 mmol s^{-1}.

For F_2 = 4.0 and 6.0 mmol s^{-1}, endpoints are reached at HI ~ 8 and 11 mmol s^{-1}, respectively. Interestingly, the yield of I atoms (i.e. the quotient of measured I atom and the known HI flow rates) is ≤ 0.5. For example, the titration endpoint in the upper panel of Figure 2b is HI ~ 11 mmol s^{-1}, but the actual measured I atom flow rate is ~6 mmol s^{-1}. The HI flow rate that defines the titration endpoint is consistent with the production of ~2 F atoms per molecule, while the actual measured I atom flow rate suggests $[F]_0 = [F_2]_0$.

Discernable endpoints were not obtained for the F + HI titrations where NF_3 was the source of the F atoms, see Figures 2c and 2d. While there appears to be a slight change in the slopes of the I vs. HI plots, a clear, well-defined plateau is not reached. The slight change in slope occurs only for the very highest HI flow rates and suggests that [F] ~ $3NF_3$, an extremely unlikely result.

The average translational temperature at x = 0 cm for both NF_3 and F_2 is 650 - 750 K. The temperature decreases to ~550 - 600 K as the flow progresses downstream.

There are several simple, potential explanations for the observed difficulties with the F + HI titrations: an ill-defined optical path length due to poor flow containment, a non-uniform vertical flow profile, or three-body and wall recombination reactions. These were all serious issues for AGIL 1, which exhibited large loss rates of atomic I along the length of the reactor as well as significant flaring of the gas flow beyond the hardware defined 5 cm path length upon ignition of the discharge. Without correction, flaring severely compromises the quality of the I atom absorption and gain measurements.

If expansion (flaring) and recirculation were important, the measured [I] should be significantly different as the flow progresses along the length of the reactor. In nearly all cases, the measured I atom flow rates were essentially identical (i.e. within 10%) from x = 0 - 10 cm. Significant variations were observed only for the lowest HI flow rates (<2 mmol s^{-1}) where a loss of approximately a factor of 2-3 was evident. For the purposes of comparison, the I atom concentration decreased by more than a factor of 3 from x = 2.5 to x = 10.5 cm for all HI flow rates in AGIL 1. A great deal of thought went into designing the AGIL 2 purge flows to prevent flow expansion and recirculation. No flaring of the flow was observed for any conditions, and the vertical profiles were consistent with plug flow. Significant wall and recombination losses are not supported by the fact that the I atom concentration is essentially constant from 0 to 10 cm at higher HI flow rates, where one would expect recombination to be more important.

The failure to measure a clear endpoint for NF_3 may be related to other factors. Secondary chemistry between NF_x and HI could conceivably generate F or I atoms in a manner that prevents a clear titration endpoint for $[HI] = [F]_0$. For example, if reaction [5]

$$NF + HI \rightarrow HNF + I \qquad [5]$$

were to occur to any significant degree, then the titration endpoint would be achieved at $[HI] = [NF_3]_0$ rather than $[HI] = [F]_0$.

All of the problems described above could also be related to the difficulty of generating and maintaining known, large flows of HI. Gaseous HI is commercially available, but the purity of the bottle contents degrades with time according to the well-known $2\ HI \leftrightarrow H_2 + I_2$ equilibrium. More seriously for large flows of HI, liquid and solid particulates may be entrained in the flow that can clog and degrade the performance of the sonic orifice. Expansion and cooling of the HI gas after passing through the orifice could lead to condensation along the tubing.

For these reasons, as well as the increasingly prohibitive cost of purchasing large quantities of high purity HI, an alternative titration method was sought and developed. Instead of flowing HI and measuring the yield of atomic I, HCl was added to the flow of F atoms and [HF] was monitored via absorption on a HF(2-0) overtone ro-vibrational transition. Because the F + HCl reaction generates a multitude of HF ro-vibrational states including significant HF(v = 2), the measured absorption signal is proportional to the population difference between HF(0,J) and HF(2,J') and the measured signal does not directly give $[F]_0$. Rather, the yield of F atoms is given by the titration endpoint. As HCl is added to the flow, the absorption signal increases until all of the F atoms are consumed and the initial F atom flow rates is given by the HCl flow necessary to reach the maximum observed signal. Large flow rates of high-purity HCl are easily (and inexpensively) generated because there are no condensation or particulate entrainment issues.

A series of F atom titrations using HCl as the titrant are shown in Figure 3. The results from these experiments complement the results from the F + HI titrations, and aid in their interpretation. While this method is not as direct or as precise as measuring [I], it is well suited to our application since we do not need a very precise endpoint and are loath to install a complicated system to deliver large flows of pure and particulate-free HI in a reliable manner.

For F_2 = 4 and 6 mmol s^{-1} (Figures 3a and 3b), the titration endpoints occur at approximately 8 and 11 mmol s^{-1} of HCl, which corresponds to 100% and 92% dissociation, respectively. The population difference signal increases as the flow progresses downstream, consistent with relaxation of vibrationally excited HF.

For NF_3 = 4.5 and 6.3 mmol s^{-1} (Figures 3c and 3d), the titration endpoints occur at approximately [HCl] = 8 and 12 mmol s^{-1} which corresponds to 1.8 and 1.9 atoms per molecule, respectively. The titration endpoints for the F + HCl titrations are much more well defined than they were for the F + HI titrations.

In Figures 3a - 3d, the translational temperature is 350 ± 30 K, significantly lower than the temperatures from the F + HI titrations. Also, unlike the F + HI titrations the temperature does not decrease significantly in the streamwise direction, but a slight upwards trend is noted with increasing HCl.

Optimization of $NCl(a^1\Delta)$

Since the small signal gain for AGIL is optimized when the density of $NCl(a^1\Delta)$ is the highest, a series of experiments were performed to determine the optimum conditions for $NCl(a^1\Delta)$ production. This was accomplished by measuring the $NCl(a^1\Delta)$ emission intensity as a function of HN_3 and DCl flow rates for constant NF_3. Sample plots are shown in Figures 4 and 5. The $NCl(a^1\Delta)$ emission spectrum was collected with a Near Infrared (NIR) Optical Multi-channel Analyzer (Roper Scientific, OMA V) attached to a 0.3 m monochromator (Acton Research Corp.). The OMA V consists of a 256 pixel array of InGaAs detectors and a well-resolved $NCl(a^1\Delta)$ spectrum with high signal to noise ratio can be collected in less than 1 second.

The conditions for Figure 4 were NF_3 = 6 mmol s^{-1}, HN_3 = 12 mmol s^{-1}, and pressure ~ 12 Torr. Two series of experiments were performed, separated in time by approximately a month. For purposes of comparison, the spectral areas are normalized to the maximum observed intensity for that experimental series. The two data series are essentially identical and the intensity of $NCl(a^1\Delta)$ reaches a plateau at approximately 12 mmol s^{-1} of DCl. Inasmuch that one would expect the $NCl(a^1\Delta)$ to optimize at the stoichiometric limit of [DCl] = [F], this tends to support the previously described F atom titration results which indicate that $[F] \sim 2[NF_3]$. Furthermore, the intensity of $NCl(a^1\Delta)$ did not decrease significantly when a nearly 2 fold excess of DCl was added. The presence of excess DCl does not appear to strongly quench $NCl(a^1\Delta)$.

In Figure 5, the NF_3 = 6 and DCl = 9 mmol s^{-1} were held constant while HN_3 was varied from 6 - 24 mmol s^{-1}. For both experiments, the maximum yield of $NCl(a^1\Delta)$ was achieved when HN_3 ~ 12 mmol s^{-1}. The Cl / HN_3 stoichiometry suggests that the optimum[28] condition for $NCl(a^1\Delta)$ production is HN_3 = 0.5Cl = NF_3, and our result is a factor of 2 too

large. This is not a surprising result considering that Herbelin[24] and Henshaw[23] reported a very similar trend for AGIL 1. Their optimum F : HN_3 ratios for gain/lasing power were 2.3 and 1.9, respectively. We attribute this difference to poor mixing. Visual inspections of the flow and computational fluid dynamics calculations support this conclusion. Future experiments to rigorously test for poor mixing are in the planning stages.

Optimization of $I^*(^2P_{1/2})$ - $I(^2P_{3/2})$ small signal gain

The results from 2 series of gain optimization experiments are shown in the upper and lower panels of Figure 6. The NF_3, DCl, and HI flow rates in the upper panel were fixed at 4.4, 16, and 0.12 mmol s^{-1}, respectively. At x = 0 and 5 cm, positive gain is observed for a relatively wide range of HN_3 flow rates. For x = 10 cm, a small absorption signal is observed in most cases. Not surprisingly, the dependence of the gain on HN_3 looks similar to the $NCl(a^1\Delta)$ optimization plot in Figure 5. For x = 0 cm the gain increases with HN_3 until a plateau is reached at approximately 20 mmol s^{-1}. The peak gain for x = 0 cm and HN_3 = 20 - 60 mmol s^{-1} is 9.0 ± 2.0 x 10^{-5} cm^{-1}. For x = 5 cm the gain increases up to 8.0 x 10^{-5} cm^{-1} for HN_3 = 20 mmol s^{-1}, but then declines with upon further additions of HN_3. A significant drop in the small signal gain occurs between 5 and 10 cm where g = 2.0 x 10^{-5} cm^{-1} is measured.

The results shown in the lower panel for NF_3 = 6,2, DCl = 25, and HI = 0.12 are qualitatively very similar. The gain increases with added HN_3 up to a peak value of 8 ± 1 x 10^{-5} cm^{-1} at ~ 35 mmol s^{-1}. As it did in the upper panel, the gain decreases along the length of the flow reactor. The peak gain at x = 5 cm is 4 ± 1 x 10^{-5} cm^{-1}. Positive small signal gain is not observed under any conditions for x = 10 cm. Surprisingly, the small signal gain for NF_3 = 6 mmol s^{-1} is lower than for NF_3 = 4 mmol s^{-1}. In principle, the maximum possible small signal gain should increase with the flow rate of F atoms. Further experimentation is required.

These results compare favorably with the AGIL 1 results; the peak gain is the same for comparable conditions. However, in contrast to the AGIL 1 results, positive gain does not persist along the length of the reactor. This difference may be related to any number of factors. First, the HI and DCl flow rates have not been optimized. While the HI flow rate is by far the smallest one, it is singularly important. According to the data in Figure 4, the DCl flow rate is not very critical. The only requirement is that $[DCl]_0 \geq [F]_0$ to prevent the formation of $NF(a^1\Delta)$.

Another critical factor that needs to be examined is the reactor pressure. For AGIL 1, the total reactor pressure upon addition of HN_3 was approximately 16 Torr. For AGIL 2, the base pressure without HN_3 was 12 Torr. Upon addition of HN_3 = 50 mmol s^{-1} (i.e. 500 mmol s^{-1} of HN_3 + He) the reactor pressure increases by a factor of 2.

Finally, a re-examination of the utility of F_2 and Cl_2 as discharge sources of F and Cl atoms, respectively should be performed. The titration plots in Figures 2 and 3 suggest that enhanced dissociation efficiency is possible with AGIL 2 and its new discharge power supplies. If sufficiently high F_2-free F atom flow rates can be generated, the gain should be comparable to, or higher than that observed in AGIL 1.

DISSCUSSION AND CONCLUSIONS

The fundamental performance characteristics of AGIL 2 have been examined. F + HI and F + HCl titrations have been used to determine the F atom production efficiency of the DC discharges. Optimum conditions for the production of $NCl(a^1\Delta)$ and $I(^2P_{1/2})$ - $I(^2P_{3/2})$ gain have been identified for a limited set of reactor conditions. To date, the highest observed small signal gain for AGIL 2 is 1.1 x 10^{-4} cm^{-1}, which is a factor of 2 smaller than the highest gain measured in AGIL 1. However, a considerable amount of parameter space remains to be explored. In particular, for a given flow rate of F atoms, the DCl and HI flows that give the highest gain have yet to be identified.

The most critical experiments that directly address the scalability of AGIL also remain to be completed. In particular, it has yet to be shown that $[NCl(a^1\Delta)]$ and gain scale with increasing [Cl]. The AGIL 1 data strongly suggested that increases in $[NF_3]$ (which leads to higher [F] and thus, higher [Cl]) leads to higher gain and higher extracted power. However, AGIL 1 was only capable of discharging $NF_3 \leq 1.5$ mmol s^{-1}, and the scaling data is limited to 2 different NF_3 flow cases (1.0 and 1.5 mmol s^{-1}). Since AGIL 2 has a larger power supply, higher NF_3 and F atom flow rates are possible. A positive correlation between [Cl] and small signal gain for a wider range of $[NF_3]$ and [Cl] would justify future AGIL scaling experiments such as the development of a supersonic AGIL device.

As a final note, small signal gain measurements have been made, but we have not (yet) attempted to extract power from the flow. We anticipate that once the operating conditions have been optimized, power levels on the order of 10's of Watts will be achieved.

ACKNOWLEDGMENTS

The authors wish to acknowledge helpful discussions with Profs. M. Heaven (Emory University) and R. D. Coombe (Denver University) regarding AGIL chemistry. We are grateful to Brian Anderson (AFRL/DE) for assistance with the diode laser. Financial support from the AFOSR is gratefully acknowledged.

REFERENCES

1. W. E. McDermott, N. R. Pchelkin, D. J. Benard and R. R. Bousek, "An Electronic Transition Chemical Laser", *Appl. Phys. Lett*, **32**, 469-470, 1978.
2. M. C. Heaven, "Chemical Dynamics in Chemical Laser Media", *Advanced Series in Physical Chemistry*, World Scientific, 2001.
3. A. C. Becker and U. Schurath, "Matrix-Isolated NCl : Radiative Rates For $b^1\Sigma^+$- $a^1\Delta$;$b^1\Sigma^+$- $X^3\Sigma^-$ and $a^1\Delta$ - $X^3\Sigma^-$ in Solid Argon", *Chem. Phys. Lett.*, **160**, 586-590, 1989.
4. D. R. Yarkony, "On the Radiative Lifetimes of the $b^1\Sigma^+$ and $a^1\Delta$ States in NCl", *J. Chem. Phys.*, **86**, 1642-1643, 1987.
5. M. Bettendorff and S. D. Peyerimhoff, "Electronic -Structure of the Radicals -NF and NCl 1. Potential-Energy Curves For NF", *Chem. Phys.*, **99**, 55-72, 1985.
6. K. B. Hewett, G. C. Manke II, D. W. Setser and G. Brewood, "Quenching Rate Constants of NCl($a^1\Delta$) at Room Temperature", *J. Phys. Chem. A.*, **104**, 539 - 551, 2000.
7. K. Y. Du and D. W. Setser, "Quenching Rate Constants of NF($a^1\Delta$) At Room-Temperature", *J. Phys. Chem.*, **94**, 2425-2435, 1990.
8. J. M. Herbelin and R. A. Klingberg, *Int. J. Chem. Kinet.*, **16**, 849, 1984.
9. G. A. Capelle, D. G. Dutton and J. I. Steinfeld, *J. Chem. Phys.*, **69**, 5140, 1978.
10. D. J. Benard, *J. Appl. Phys.*, **74**, 2900, 1993.
11. D. J. Benard and B. K. Winker, *J. Appl. Phys.*, **69**, 2805, 1991.
12. D. J. Benard, B. K. Winker, T. A. Seder and R. H. Cohn, *J. Phys. Chem.*, **93**, 4790, 1989.
13. D. J. Benard, E. Boehmer, H. H. Michels and Jr. J. A. Montgomery, *J. Phys. Chem.*, **98**, 8952, 1994.
14. E. Boehmer and D. J. Benard, *J. Phys. Chem.*, **99**, 1969, 1995.
15. D. J. Benard and E. Boehmer, *Appl. Phys. Lett.*, **65**, 1340, 1994.
16. D. J. Benard, *J. Phys. Chem.*, **100**, 8316, 1996.
17. K. Y. Du and D. W. Setser, "Quenching Reactions of NF($a^1\Delta$) By Cl_2 ; ClF ; Br_2 ; ICl ; IF ; and I_2", *J. Phys. Chem.*, **96**, 2553-2561, 1992.
18. D. W. Setser, unpublished results, 2000
19. G. C. Manke II, *to be published*, 2002.
20. H. Cha and D. W. Setser, "NF($b^1\Sigma^+$) Quenching Rate Constants By Halogens and Interhalogens and the Excitation Rate-Constant For IF(B) Formation", *J. Phys. Chem.*, **91**, 3758-3767, 1987.
21. A. J. Ray and R. D. Coombe, "Energy-Transfer From NCl($a^1\Delta$) to Iodine Atoms", *J. Phys. Chem.*, **97**, 3475-3479, 1993.
22. T. L. Henshaw, S. D. Herrera and L. A. V. Schlie, "Temperature-Dependence of the Ncl($a^1\Delta$)+I($^2P_{3/2}$) Reaction From 300 to 482 K", *J. Phys. Chem. A*, **102**, 6239-6246, 1998.
23. Thomas L. Henshaw, Gerald C. Manke II, Timothy J. Madden, Michael R. Berman and Gordon D. Hager, "A new energy transfer chemical laser at 1.315 μm", *Chem. Phys. Lett.*, **325**, 537 - 544, 2000.
24. J. M. Herbelin, T. L. Henshaw, B. D. Rafferty, B. T. Anderson, R. F. Tate, T. J. Madden, G. C. Manke and G. D. Hager, "The measurement of gain on the 1.315 μm transition of atomic iodine in a subsonic flow of chemically generated NCl($a^1\Delta$)", *Chem. Phys. Lett.*, **299**, 583-588, 1999.
25. R. D. Bower and T. T. Yang, "I($^2P_{1/2}$) Produced By the Energy-Transfer From Ncl($a^1\Delta$) to I($^2P_{3/2}$)", *J. Opt. Soc. Am. B*, **8**, 1583-1587, 1991.
26. A. J. Ray and R. D. Coombe, "An I* Laser-Pumped By NCl($a^1\Delta$)", *J. Phys. Chem.*, **99**, 7849-7852, 1995.
27. G. C. Manke II, T. L. Henshaw, T. J. Madden, J. M. Herbelin, B. D. Rafferty and G. D. Hager, "Characterizing fluorine and chlorine atom flow rates using iodine atom spectrometry", *AIAA Journal*, **39**, 447 - 454, 2001.
28. G. C. Manke II and D. W. Setser, "Kinetics of NCl($a^1\Delta$ and $b^1\Sigma^+$) Generation: The Cl + N_3 Rate Constant, the NCl($a^1\Delta$) Product Branching Fraction , and Quenching of NCl($a^1\Delta$) by F and Cl Atoms", *J. Phys. Chem. A*, **102**, 7257-7266, 1998.

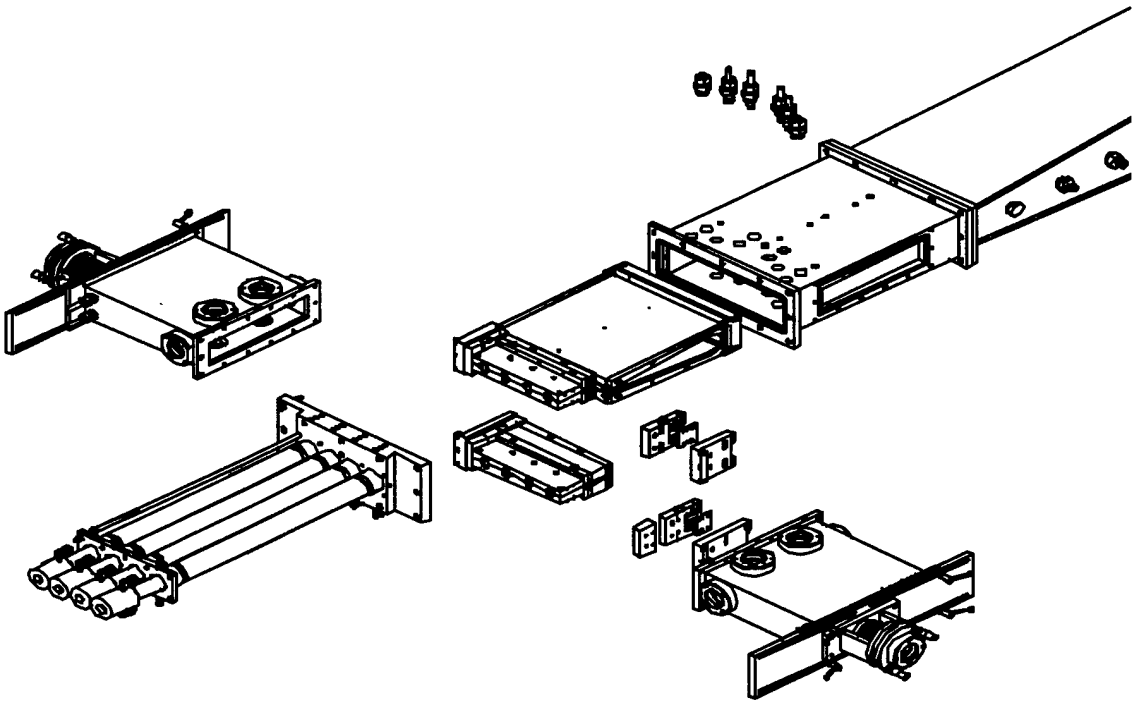

Figure 1. Construction schematic for AGIL 2. Major components include the 4 discharge tubes with radial He and DCl injectors attached to the ends, HI and HN_3 injector blocks, flow reactor with adjustable ramps, He injectors for containment of the flow, and laser mirror tunnels and mounts.

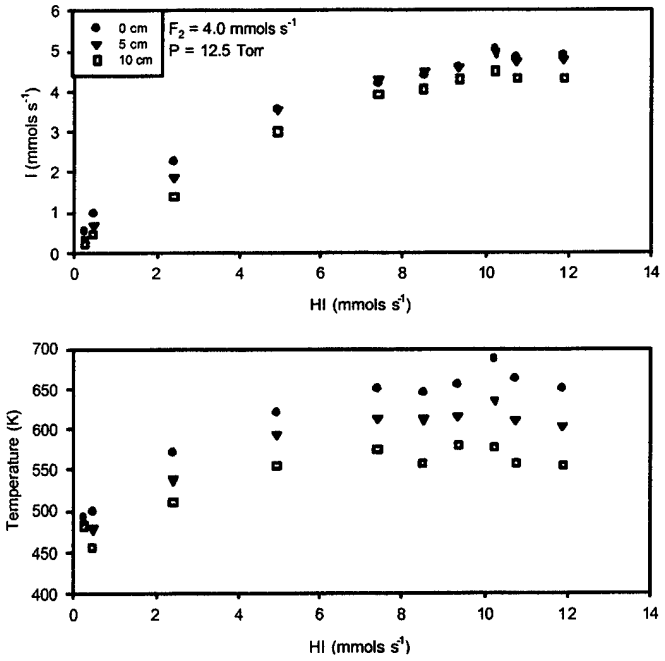

Figure 2a. F + HI Titrations for F_2 = 4 mmol s^{-1}

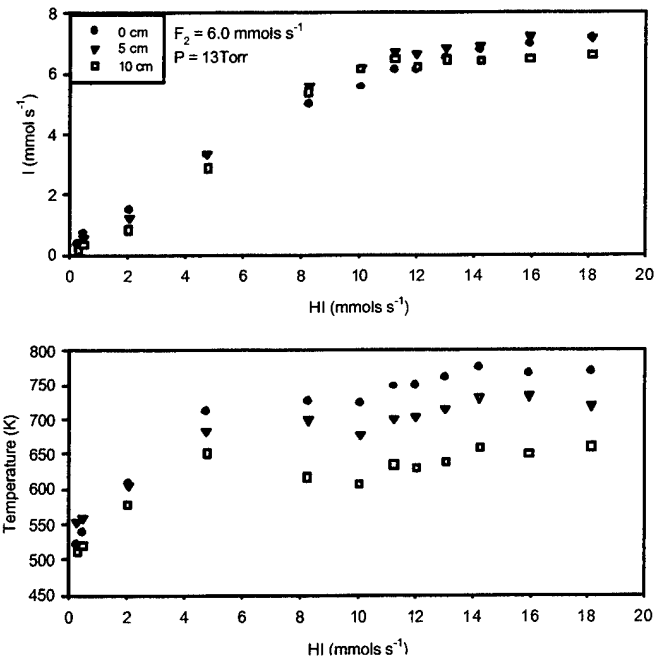

Figure 2b. F + HI Titrations for F_2 = 6 mmol s^{-1}

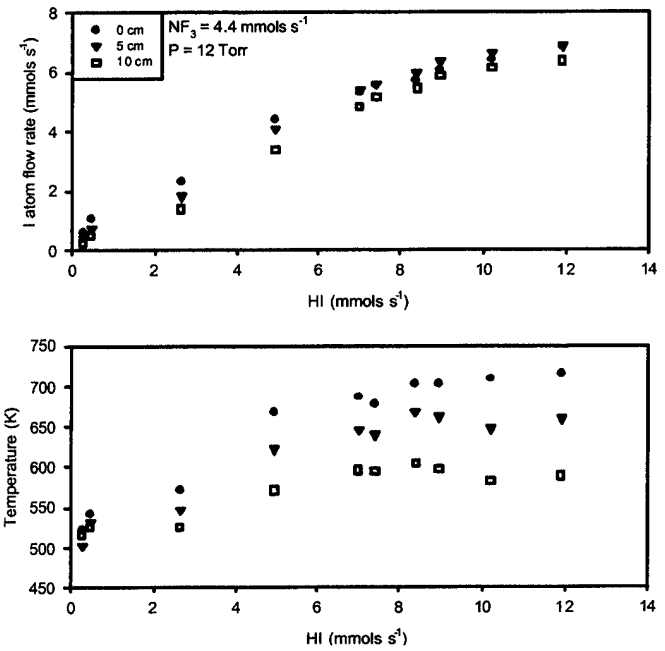

Figure 2c. F + HI Titrations for NF_3 = 4.4 mmol s^{-1}

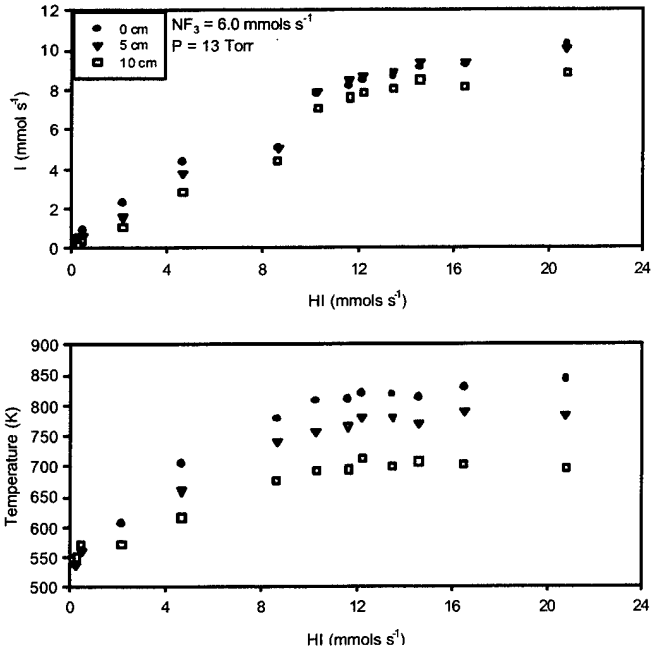

Figure 2d. F + HI Titrations for NF_3 = 6 mmol s^{-1}

Figure 2. F + HI titrations. The upper plot in each panel shows the flow rate of atomic iodine as a function of added HI, while the lower plot in each panel shows the temperature variation with added HI. In all cases, the various symbols indicate different downstream positions: ● = 0 cm, ▼ = 5 cm, and = 10 cm downstream from the end of the HI / HN_3 injector blocks.

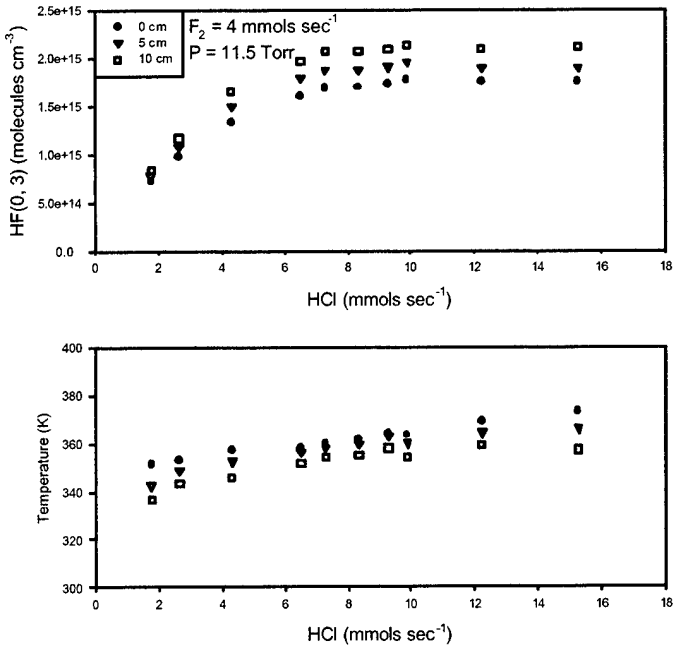

Figure 3a. F + HCl Titrations for F_2 = 4 mmol s^{-1}

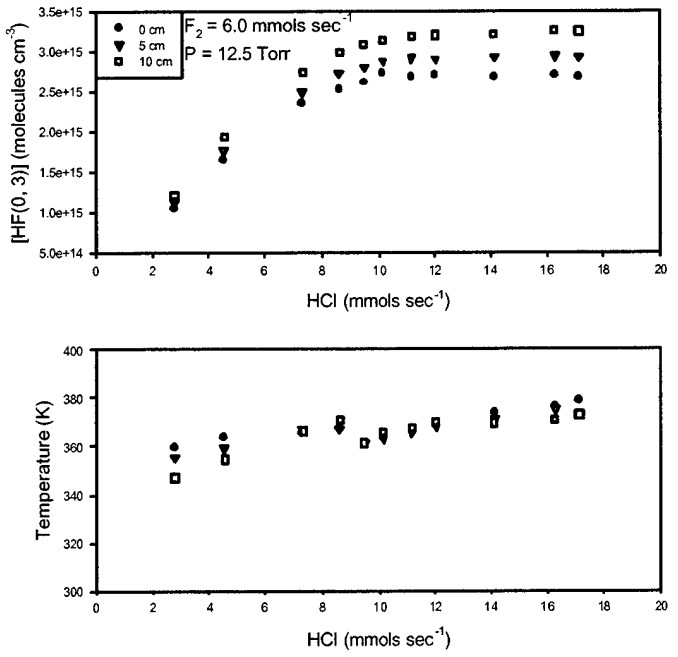

Figure 3b. F + HCl Titrations for F_2 = 6 mmol s^{-1}

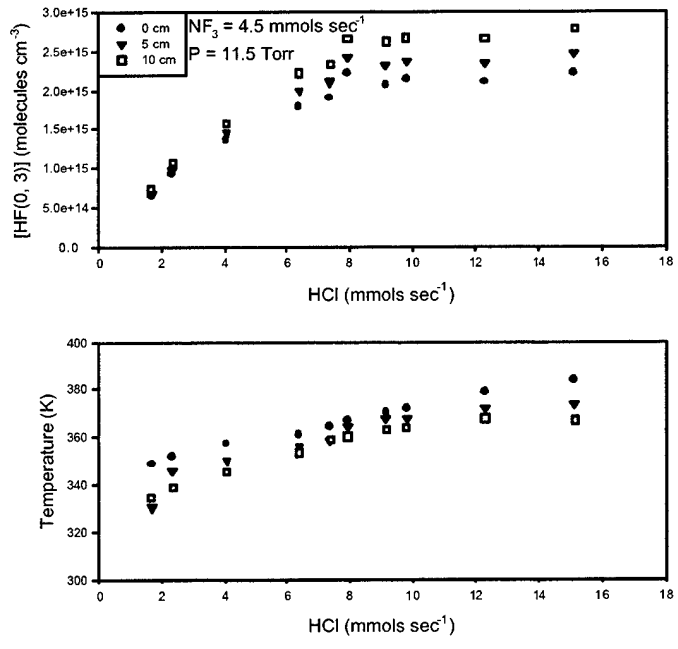

Figure 3c. F + HCl titrations for NF_3 = 4 mmol s^{-1}

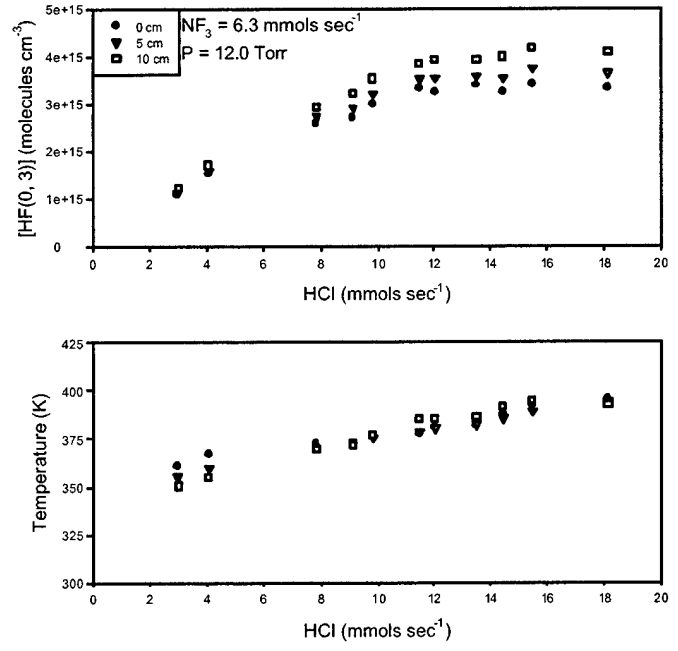

Figure 3d. F + HCl titrations for NF_3 = 6 mmol s^{-1}

Figure 3. F + HCl titrations. The upper plot in each panel shows the measured population difference ([HF(0,3)] - 5/7[HF(2,4)]) as a function of added HCl, see text for details. The lower plot in each panel shows the variation in temperature with added HCl. In all cases, the various symbols indicate different downstream positions: ● = 0 cm, ▼ = 5 cm, and □ = 10 cm downstream from the end of the HI / HN_3 injector blocks.

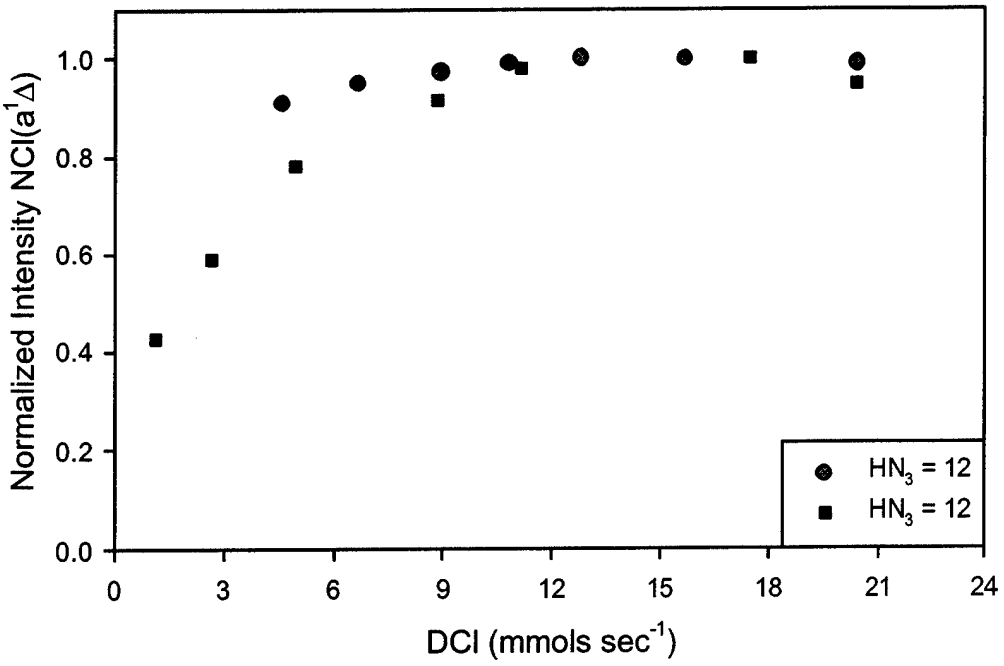

Figure 4. Optiimization of NCl(a$^1\Delta$) density vs. DCl. The NF_3 flow rate used for these was 6 mmol s^{-1}. The emission intensity of NCl(a$^1\Delta$) is optimized at DCl = 12 mmol s^{-1}, consistent with the expectation that NCl(a$^1\Delta$) production is optimal when [DCl] = [F] = 2[NF_3], and all of the F atoms have been consumed.

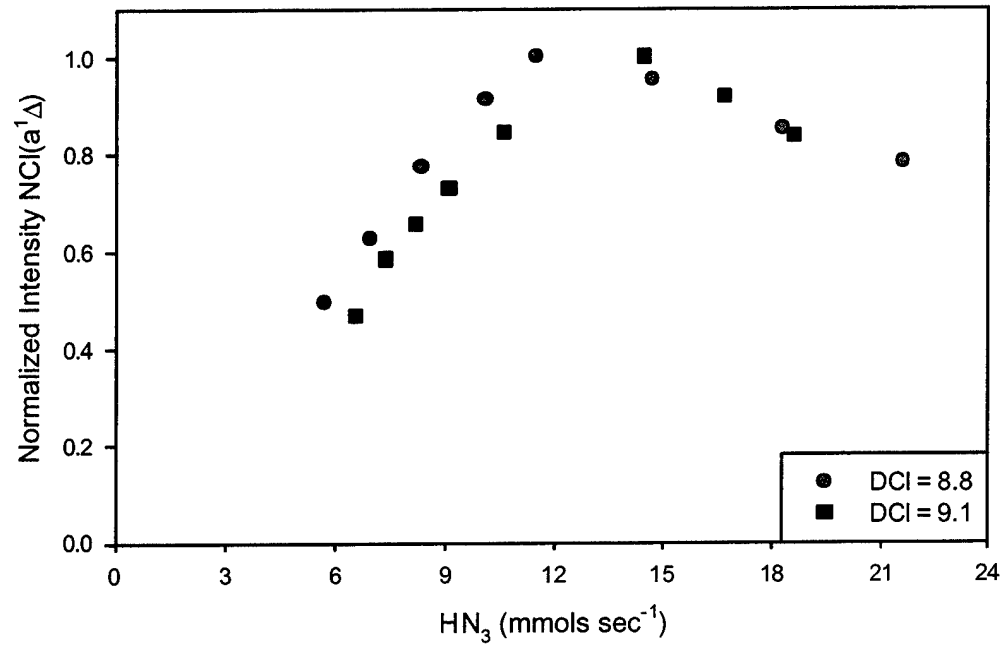

Figure 5. Optiimization of NCl(a$^1\Delta$) density vs. HN_3. The NF_3 flow rate used for these experiments was 6 mmol s^{-1}. The emission intensity of NCl(a$^1\Delta$) is optimized at HN_3 = 12 mmol s^{-1}. According to the stoichiometry of the F / DCl / HN_3 chemical mechanism for the formation of NCl(a$^1\Delta$), the density of NCl(a$^1\Delta$) should be optimized at [HN_3] = 0.5[F] = [NF_3] rather than the 2 - 3 fold excess of HN_3 shown above.

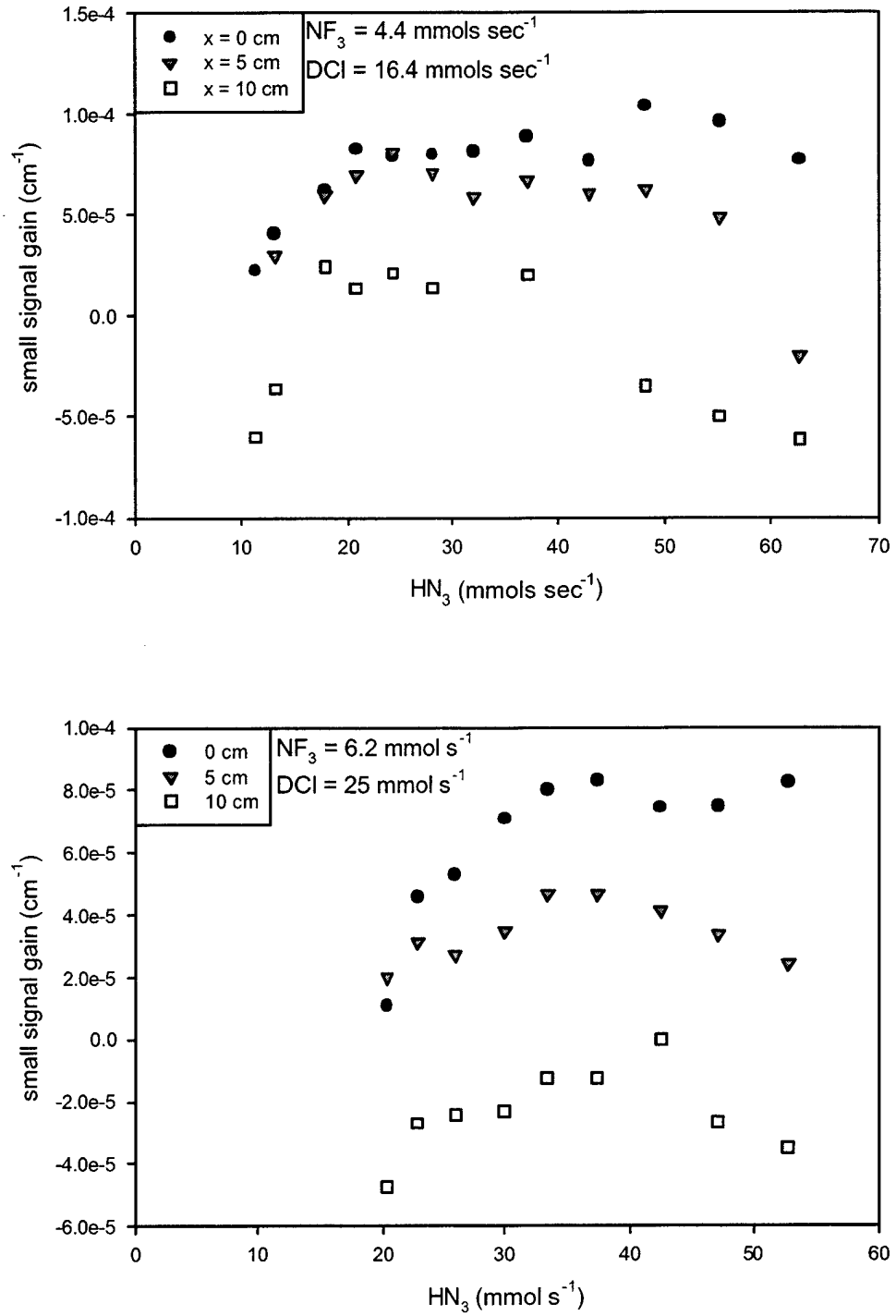

Figure 6. Small signal gain optimization. According to the stoichiometry of the F / DCl / HN_3 chemical mechanism for the formation of $NCl(a^1\Delta)$, the density of $NCl(a^1\Delta)$ should be optimized at $[HN_3] = 0.5[F] = [NF_3]$ rather than the 2 - 3 fold excess of HN_3 observed in the plots above. Similar trends were noted by Henshaw and co-workers in their gain optimization experiments for AGIL 1.